ISSN 1029-9599, Physical Mesomechanics, 2024, Vol. 27, No. 4, pp. 426–435. © Pleiades Publishing, Ltd., 2024.
Russian Text © The Author(s), 2024, published in Fizicheskaya Mezomekhanika, 2024, Vol. 27, No. 2, pp. 112–123.

Grain Interaction and Elastic Strain Distribution in Polycrystalline Materials

V. E. Shavshukov

Perm National Research Polytechnic University, Perm, 614990 Russia
e-mail: shavshukov@pstu.ru

Received August 22, 2023; revised October 18, 2023; accepted November 4, 2023

Abstract—Statistical distributions of the elastic strain and stress tensor components in the grains of polycrystalline materials are necessary to calculate the probabilities of various local critical events, such as damage and others, which are of random origin due to the stochastic grain structure. Many experimental and computational studies suggest that these distributions can be approximated by a normal distribution. The normal distribution parameters are determined from histogram-like plots obtained experimentally or by computer simulation. Most published histogram distributions are highly skewed, in contrast to the normal distribution. Here we present a new direct calculation method for the probability densities of the elastic strain tensor components. The method uses an integral equation for strains in heterogeneous solids, which reduces the solution of the boundary value problem of polycrystal deformation to the sum of solutions of some problems for neighboring grains. The focus is on the influence of random grain interactions on the strain distribution. Calculations are carried out for polycrystals with different elastic symmetries and degrees of grain anisotropy. All probability densities are finite, asymmetric, and noticeably different from Gaussian ones. It is shown that very few particularly located neighboring grains (of dozens) have a much greater effect on the distribution pattern and limiting values of the strain tensor components than all the others.

Keywords: polycrystalline materials, stochastic mesostrain fields, strain distributions

DOI: 10.1134/S1029959924040076

1. INTRODUCTION

Polycrystalline materials are the most common structural materials. They have a stochastic grain structure, i.e. the shape and size of grains as well as the orientation of their crystallographic axes are random. As a result, the strain fields as a function of coordinates in polycrystalline solids are highly nonuniform both in neighboring grains and inside individual grains. They are also stochastic due to random grain structures in polycrystals. These fields can be studied either as random functions of coordinates in a specific macroscopic specimen, or as random variables at a fixed point using an ensemble of grain structure configurations. Within the ergodic hypothesis, these approaches are equivalent. In this work, the method of statistical ensembles is used.

The macroscopic mechanical response of a polycrystalline solid to external action is the result of the cooperative behavior of a very large number of grains that constitute the polycrystal. It is generally accepted that the nonuniformity of mechanical fields on the scale of individual grains (mesoscale) during deformation is the driving force behind local damage, damage accumulation, and subsequent macrofracture. Knowledge of the behavior of polycrystalline materials on the mesoscale and its dependence on various structural factors is needed for a fundamental understanding of the stochastic processes of deformation and fracture of polycrystalline solids. Knowledge of the distribution functions of the components of the fluctuating strain and stress fields is basic, for example, to the calculation of damage probabilities, which occur in grains with the maximum strain and stress tensor component or their combinations in accordance with certain criteria.

The statistical characteristics of nonuniform strain fields in polycrystalline materials can be studied both experimentally and numerically. An experimental study of intragranular strain inhomogeneity can be carried out by the high-resolution digital image correlation method [1, 2] for surface grains and by the synchrotron X-ray diffraction method and X-ray mic-

rotomography for subsurface grains of a polycrystalline solid [3–8].

The most common computational investigation includes development of a three-dimensional geometric model of the polycrystalline structure and numerical solution of the corresponding boundary value problem. Methods of reproducing real grain structures in this or that models (of shapes, equilibrium angles of triple junctions, crystallographic orientation of grains, etc.) have been intensively developed in recent decades. Early and relatively recent methods were reviewed in [9, 10]. New methods are based on step-by-step packing of a representative volume [11], consideration for the experimental data to optimize the synthesized grain structures of polycrystals [12], etc. Boundary-value problems of deformation of the built structures are most often solved by the finite element method. For this purpose, geometric models are integrated into any computational package (for example, ABAQUS/Explicit) [13, 14], or special software is developed for them (for example, [15]). Another computational approach to studying the deformation of polycrystalline materials is based on the method of internal variables. This method provides no explicit description of the grain structure geometry, but introduces new phenomenological variables, which are given by evolution relations. The method is multilevel and is applicable to scale levels from the macroscopic to dislocation one. The method and its applications are detailed in [16].

The experimental and computational approaches study random strain fields on discrete statistical samples (dataset) of strain tensor components measured in polycrystal grains or taken at the finite element intersections from the solution of a boundary value problem for model polycrystals. Statistical distributions are plotted based on the frequency of falling of random values of the samples into the specified intervals of random variables. The distributions thus obtained have a histogram form [17–21]. For a continuous representation, such densities are interpolated by some model distributions. For elastic strains, the normal distribution is usually used, which is symmetric with respect to the average random variable. However, histogram distributions published so far often have noticeable visual asymmetries [17–21]. This paper proposes an alternative method for calculating distributions, which establishes the causes of deviations from the Gaussian distribution.

The randomness of strains is due to the randomness of shapes and crystallographic orientations of grains, as well as due to their random interactions. It was experimentally established that the interaction of neighboring grains has a strong influence on the strain in individual grains in terms of its inhomogeneity and stochasticity [22]. Among all factors, the mutual orientation of the crystallographic axes of the interacting grains has a decisive influence on mesostrain. This work focuses on this stochastic factor, i.e. random interactions of grains caused by the random orientation of their crystallographic axes. Other random factors, such as foreign inclusions, inhomogeneities in the chemical composition (for alloys), different modifications of grains, residual stresses, and other features of commercial polycrystalline materials are given no consideration. We deal only with single-phase polycrystals consisting of grains of the same type. All strains are assumed to be low, so that no irreversible changes occur in the structure during deformation. The statistical strain distribution is calculated by the method of integral equations for the strain tensor in heterogeneous solids modified for the case of polycrystals. The specific structure of the equations for a polycrystalline solid made it possible to develop an effective method for solving these equations and to process a large number of implementations of random structures for the statistical analysis of random strains.

The work shows that the statistical strain distributions are non-Gaussian, that the influence of the interaction on the strain tensor components in any grain of a polycrystal is significantly different for the neighboring grains, and that this causes the deviation of the studied distributions from the normal distribution.

2. INTEGRAL EQUATION FOR MESOSTRAINS IN GRAINS

The integral equation for the strain tensor $\varepsilon_{mn}(\mathbf{r})$ in large heterogeneous macroscopically isotropic solids (for which the surface integral usually present in such equations tends to 0) was differently written [23–25, etc.] and has the form

$$\varepsilon_{mn}(\mathbf{r}) = \varepsilon^{*}_{mn}(\mathbf{r}) + \int_V g_{mnij}(\mathbf{r}-\mathbf{r}')[C_{ijkl}(\mathbf{r}') - \langle C_{ijkl}\rangle]\varepsilon_{kl}(\mathbf{r}')\mathrm{d}^3\mathbf{r}', \quad (1)$$

where $C_{ijkl}(\mathbf{r})$ is the coordinate-dependent elastic modulus tensor determined over the entire volume of the solid, and $\langle C_{ijkl}\rangle$ is the isotropic elastic modulus tensor averaged over the solid volume V:

$$\langle C_{ijkl}\rangle \equiv 1/V \int_V C_{ijkl}(\mathbf{r})\mathrm{d}\mathbf{r},$$

$g_{mnij}(\mathbf{r})$ is Green's tensor of an isotropic averaged medium with the elastic modulus tensor $\langle C_{ijkl}\rangle$, and $\varepsilon^*_{mn}(\mathbf{r})$ is the macrostrain tensor components obtained from the solution of the boundary value problem for an averaged homogeneous solid, which is assumed to be known. Summation is performed over repeated subscripts in (1).

Integral Eq. (1) is derived from differential equations for the two boundary value problems in displacements: a boundary value problem for a solid with the averaged elastic modulus tensor and a boundary value problem for a heterogeneous solid. The transition from differential to integral equations is implemented by introducing Green's tensor [24]. Both solids are of the same shape and size. External loads are specified by assigning displacements to all boundary points. Consequently, the boundary conditions for both problems are chosen to be kinematic: displacements $u_i(\mathbf{r})\big|_\Gamma = \varphi_i(\mathbf{r})$ are specified on the external surfaces of the solids, where $\varphi_i(\mathbf{r})$ is the specified functions that are the same for both solids, and Γ is the solid surface. Below we consider only the case of macroscopically uniform deformation of both solids. For an averaged solid, this means that $\varepsilon^*_{mn}(\mathbf{r})$ is the coordinate-independent constant ε^*_{mn}. It corresponds to homogeneous displacement boundary conditions, where x_n is the projections of the radius-vector $\mathbf{r}$ on the coordinate axes. In this particular case, there is no need to solve the problem for a homogeneous solid. The components are found immediately from the boundary conditions. For a heterogeneous solid under the same boundary conditions, the strain averaged over the solid volume is given by [24]

$$\langle \varepsilon_{mn}\rangle \equiv 1/V \int_V \varepsilon_{mn}(\mathbf{r})\mathrm{d}\mathbf{r} = \varepsilon^*_{mn}.$$

For a macroscopically homogeneous polycrystalline solid under uniform deformation, the strain tensor averaged over the representative volume coincides with that averaged over the solid volume. The introduction of a solid with averaged properties (reference solid) is a mathematical technique that makes it possible to separate the influence of boundary conditions (only ε^*_{mn} depend on them) and heterogeneities (the term with the volume integral, which is independent of the boundary conditions) on the solution of Eq. (1). Equation (1), its variables, as well as all the following expressions and variables refer to the single laboratory coordinate system of the solid. Green's tensor has the known form [24]

$$g_{ijkl}(\mathbf{r}) = -\frac{1}{3\langle\mu\rangle}\left[(1-\chi)V_{ijkl} + \left(1-\frac{2}{5}\chi\right)D_{ijkl}\right]\delta(\mathbf{r}) + \frac{f_{ijkl}(\mathbf{r})}{\langle\mu\rangle\,|\,\mathbf{r}\,|^3},$$

where $\chi = (3\langle K\rangle + \langle\mu\rangle)/(3\langle K\rangle + 4\langle\mu\rangle)$ is the material parameter, $\langle K\rangle$ and $\langle\mu\rangle$ are the averaged bulk modulus and shear modulus of the homogenized medium, δ_{ij} is the Kronecker delta symbol, V_{ijkl} and D_{ijkl} are the spherical and deviatoric parts of the unit tensor $I_{ijkl} = 1/2(\delta_{ik}\delta_{jl} + \delta_{il}\delta_{jk})$, and $\delta(\mathbf{r})$ the Dirac delta function. The function $f_{ijkl}(\mathbf{r})$ depends only on the angles between the radius-vector $\mathbf{r}$ and the coordinate axes:

$$f_{ijkl}(\mathbf{r}) = \frac{1}{8\pi}[3(n_i n_l\delta_{jk} + n_j n_l\delta_{ik}) - 2I_{ijkl} + \chi(I_{ijkl} + I_{ikjl} + I_{iljk}) - 3\chi(n_i n_j\delta_{kl} + n_i n_k\delta_{jl} + n_i n_l\delta_{jk} + n_j n_k\delta_{il} + n_j n_l\delta_{ik} + n_k n_l\delta_{ij} - 5n_i n_j n_k n_l)],$$

where $n_i = x_i/|\,\mathbf{r}\,|$ is the direction cosines of the radius-vector $\mathbf{r}$ (x_i is the projection of the radius-vector on the ith coordinate axis). The variables without superscripts and referring to the whole solid are called global variables.

Equation (1) is applicable to any type of heterogeneous solids. In polycrystalline solids, the components of the global elastic modulus tensor $C_{ijkl}(\mathbf{r})$ are rapidly oscillating functions of coordinates. They are constant inside a grain and change abruptly in transition to another grain due to rotation of the crystallographic axes of the grains or different grain types (in multiphase polycrystals). Below, we study only single-phase polycrystals consisting of grains of the same type. With this in mind, it is convenient to decompose global field variables into the sums of local (mesoscopic) fields using the indicator functions $\lambda_\xi(\mathbf{r})$ (equal to 1 in the ξth grain and 0 in other cases). For the global elastic modulus and strain tensors, we have

$$C_{ijmn}(\mathbf{r}) = \sum_{\xi=1}^{N}\lambda_\xi(\mathbf{r})C^{(\xi)}_{ijmn}(\mathbf{r}), \quad (2)$$

$$\varepsilon_{ij}(\mathbf{r}) = \sum_{\xi=1}^{N}\lambda_\xi(\mathbf{r})\varepsilon^{(\xi)}_{ij}(\mathbf{r}). \quad (3)$$

Hereinafter, Greek superscripts and subscripts (ξ, η, etc.) number grains of the polycrystal, N is the total number of grains in the polycrystal (macroscopically large number), $C^{(\xi)}_{ijmn}(\mathbf{r})$ and $\varepsilon^{(\xi)}_{ij}(\mathbf{r})$ are the tensors of elastic moduli and strains of the ξth grain in the la-

boratory coordinate system, the domain of which is the volume of the ξth grain. The superscript distinguishes local variables from global ones.

Using Eqs. (2) and (3) for polycrystalline solids, Eq. (1) is transformed into the system of equations for local strain tensors $\varepsilon_{ij}^{(\xi)}(\mathbf{r}_\xi)$ in each grain [26]

$$\varepsilon_{ij}^{(\xi)}(\mathbf{r}_\xi) = \varepsilon_{ij}^* + \int\limits_{\omega_\xi} \mathrm{d}\mathbf{r}'_\xi g_{ijkl}(\mathbf{r}_\xi - \mathbf{r}'_\xi)(C_{klmn}^{(\xi)}(\mathbf{r}'_\xi) - \langle C_{klmn}\rangle)\varepsilon_{mn}^{(\xi)}(\mathbf{r}'_\xi) + \sum_{\eta\neq\xi}^{N} \int\limits_{\omega_\eta} \mathrm{d}\mathbf{r}'_\eta g_{ijkl}(\mathbf{r}_\xi - \mathbf{r}'_\eta)(C_{klmn}^{(\eta)}(\mathbf{r}'_\eta) - \langle C_{klmn}\rangle)\varepsilon_{mn}^{(\eta)}(\mathbf{r}'_\eta), \quad (4)$$

where ω_ξ, and ω_η are the volumes of the ξth and ηth grains. The subscript of the radius-vector $\mathbf{r}_\xi$ indicates that it varies only within the ξth grain.

System (4) consists of a huge number of equations equal to the number of grains in the solid. It can be interpreted in terms of the interaction of strains at different points of the solid. The first integral on the right-hand side of (4) describes the influence of strains at all points inside the ξth grain on the strain at a given point $\mathbf{r}_\xi$ of this grain. One can say that this integral represents the intragranular strain interaction. Each integral under the summation sign in (4) represents the influence of strains at all points inside the ηth grain on the strain of the studied grain (the ξth one) at a given point $\mathbf{r}_\xi$. The entire sum represents the effect of intergranular interactions of all grains in a polycrystalline solid with the studied grain. Thus, a polycrystalline solid is represented as a system of interacting grains.

Solving the system of integral Eqs. (4) is a difficult task. An approximate solution can be derived by using a piecewise constant approximation for the $\varepsilon_{ij}^{(\xi)}(\mathbf{r})$ fields. To do this, we divide each grain into a sufficiently large number of small subregions so that strains within each subregion can be considered approximately constant and change in steps in transition to the neighboring subregion. For brevity, these subregions are called subgrains. Within the same grain, they are physically no different, i.e. they have the same elastic moduli and crystallographic orientations. Let us decompose intragranular strains $\varepsilon_{ij}^{(\xi)}(\mathbf{r}_\xi)$ in all grains into the sums of subgrain strains $\varepsilon_{ij}^{(a)(\xi)}$ using the indicator functions:

$$\varepsilon_{ij}^{(\xi)}(\mathbf{r}_\xi) = \sum_{a=1}^{n} \lambda_a(\mathbf{r}_\xi)\varepsilon_{ij}^{(a)(\xi)},$$

$$\varepsilon_{ij}^{(\eta)}(\mathbf{r}_\eta) = \sum_{e=1}^{n} \lambda_e(\mathbf{r}_\eta)\varepsilon_{ij}^{(e)(\eta)}, \quad (5)$$

where $\lambda_a(\mathbf{r}_\xi)$ is the indicator function of the *a*th subgrain in the ξth grain (equal to 1 inside the subgrain and 0 otherwise), $\lambda_e(\mathbf{r}_\eta)$ is the indicator function of the *e*th subgrain in the ηth grain, and *n* is the number of subgrains in each grain. Hereinafter, Latin superscripts and subscripts number subgrains in the grain, and Greek ones, as mentioned above, number grains. Strains $\varepsilon_{ij}^{(a)(\xi)}(\mathbf{r}_\xi)$ and $\varepsilon_{ij}^{(e)(\eta)}(\mathbf{r}_\eta)$ are constant within the corresponding subgrains. This procedure transforms the system of integral Eqs. (4) into the system of linear algebraic equations for subgrain strains $\varepsilon_{ij}^{(a)(\xi)}$ in all polycrystal grains [27]

$$[I_{ijmn} - B_{ijmn}^{(aa)(\xi)}]\varepsilon_{ij}^{(a)(\xi)} = \varepsilon_{ij}^* + \sum_{b\neq a}^{n} B_{ijmn}^{(ab)(\xi)}\varepsilon_{mn}^{(b)(\xi)} + \sum_{\eta\neq\xi}^{N}\sum_{e=1}^{n} B_{ijmn}^{(ae)(\eta)}\varepsilon_{mn}^{(e)(\eta)}, \quad (6)$$

where the dimensionless tensor coefficients

$$B_{ijmn}^{(ab)(\xi)} \equiv \int\limits_{\omega_b} \mathrm{d}\mathbf{r}'_b g_{ijkl}(\mathbf{r}_a - \mathbf{r}'_b)\cdot C_{klmn}'^{(\xi)}, \quad B_{ijmn}^{(ae)(\eta)} \equiv \int\limits_{\omega_e} \mathrm{d}\mathbf{r}'_e g_{ijkl}(\mathbf{r}_a - \mathbf{r}'_e)\cdot C_{klmn}'^{(\eta)} \quad (7)$$

characterize the intensity of subgrain interactions. In (6) and (7), the subscripts *a* and *b* number subgrains of the ξth grain, the subscript *e* numbers subgrains of the ηth grain, $\omega_{b(\xi)}$ and $\omega_{e(\eta)}$ are the subgrain volumes. The first coefficient describes the interaction of subgrains in the same grain, and the second one describes the interaction of subgrains in different grains.

System (6) consists of $n\times N$ equations, being much larger than system (4). It is solved using perturbation theory. All subgrain interactions, i.e. both terms with the summation signs in (6) are considered as a perturbation. The solution is represented as an infinite sum of corrections of all orders

$$\varepsilon_{ij}^{(a,b,e)(\xi,\eta)}(\mathbf{r}) = \varepsilon_{ij}^{(0)(a,b,e)(\xi,\eta)}(\mathbf{r}) + \varepsilon_{ij}^{(1)(a,b,e)(\xi,\eta)}(\mathbf{r}) + \varepsilon_{ij}^{(2)(a,b,e)(\xi,\eta)}(\mathbf{r}) + \ldots, \quad (8)$$

and the corrections satisfy an infinite chain of the coupled subsystems of equations

$$\varepsilon_{ij}^{(0)(a)(\xi)} - B_{ijkl}^{(aa)(\xi)}\varepsilon_{kl}^{(0)(a)(\xi)} = \varepsilon_{ij}^*,$$

$$\varepsilon_{ij}^{(1)(a)(\xi)} - B_{ijkl}^{(aa)(\xi)}\varepsilon_{mn}^{(1)(a)(\xi)} = \sum_{b\neq a}^{n} B_{ijkl}^{(ab)(\xi)}\varepsilon_{kl}^{(0)(b)(\xi)} + \sum_{\eta\neq\xi}\sum_{e=1}^{n} B_{ijkl}^{(ae)(\eta)}\varepsilon_{kl}^{(0)(e)(\eta)}, \quad (9)$$

$$\varepsilon_{ij}^{(2)(a)(\xi)} - B_{ijkl}^{(aa)(\xi)}\varepsilon_{mn}^{(2)(a)(\xi)}$$
$$= \sum_{b\neq a}^{n} B_{ijkl}^{(ab)(\xi)}\varepsilon_{kl}^{(1)(b)(\xi)} + \sum_{\eta\neq\xi}\sum_{e=1}^{n} B_{ijkl}^{(ae)(\eta)}\varepsilon_{kl}^{(1)(e)(\eta)} \text{ etc.}$$

For most real polycrystals, all $|B_{ijmn}^{(ab)(\xi)}|$ and $|B_{ijmn}^{(ae)(\eta)}|$ are of the order 10^{-2} or less, and $|B_{ijmn}^{(ae)(\eta)}| \ll |B_{ijmn}^{(ab)(\xi)}|$. In the first-order approximation for the subgrain interaction $B_{ijmn}^{(ab)(\xi)}$ and $B_{ijmn}^{(ae)(\eta)}$, the solution is reduced to the sum of the zero-order and first-order corrections: (details in [27]):

$$\varepsilon_{ij}^{(a)(\xi)} \cong \varepsilon_{ij}^{(0)(a)(\xi)} + \varepsilon_{ij}^{(1)(a)(\xi)}, \tag{10}$$

and the corrections satisfy the equations

$$\varepsilon_{ij}^{(0)(a)(\xi)} = \varepsilon_{ij}^{*} + B_{ijkl}^{(aa)(\xi)}\varepsilon_{kl}^{(0)(a)(\xi)},$$
$$\varepsilon_{ij}^{(1)(a)(\xi)} = \left(\sum_{\eta\neq\xi}\tilde{B}_{ijkl}^{(a\eta)}\right)\varepsilon_{kl}^{*}, \tag{11}$$

where the new coefficient

$$\tilde{B}_{ijmn}^{(a\eta)} \equiv \int_{\omega_\eta} \mathrm{d}\mathbf{r}'_\eta g_{ijkl}(\mathbf{r}_a - \mathbf{r}'_\eta)\cdot(C_{klmn}^{(\eta)} - \langle C_{klmn}\rangle) \tag{12}$$

determines the intensity of interaction of the ath subgrain in the ξth grain with the entire ηth grain integrally. The solution of (11) depends on the polycrystal structure through $B_{ijkl}^{(aa)(\xi)}$ and the entire sum in the brackets of (11).

3. ADDITIVITY OF INTERACTIONS AND LARGE RANDOM SAMPLES OF GRAIN STRUCTURE IMPLEMENTATIONS

A particular polycrystalline specimen has a fixed grain structure. Consequently, Eqs. (11) give a deterministic mesostrain value at any given point inside the solid. To trace the mesostrain randomness depending on the coordinates, we use the ergodic hypothesis. According to this hypothesis, it is necessary to fix the point $\mathbf{r}_a$, to generate a large number of random implementations of the grain structure for the entire polycrystal, and to solve system (11) for each implementation. The obtained solutions constitute a set of possible random mesostrains for the entire polycrystal. This value set can be used to build the mesostrain distribution. Since the set of possible structure implementations is continuously large, the number of implementations must be very large to be statistically sufficient.

Random factors in system (11) are the coefficients $B_{ijkl}^{(aa)(\xi)}$ and $\tilde{B}_{ijmn}^{(a\eta)}$. They determine the stochastic nature of the problem of determining random mesostrains. The summands of (11) determine the influence of each individual polycrystal grain on the solution in the studied ξth grain and make it independently. Mathematically, the influence of grain interactions on the solution is additive. Moreover, the solution does not depend on the boundary conditions for a polycrystalline solid. Boundary conditions determine only the macrostrain in the averaged solid ε_{ij}^{*}. The second equation in (11) shows that we deal with a multiplicative expansion of two factors influencing the solution: boundary conditions and polycrystalline structure. Only the first factor (the sum in the parentheses) is random. If a sufficiently large number of the coefficients $\tilde{B}_{ijmn}^{(a\eta)}$ is calculated, the model calculations correspond to a macroscopic polycrystalline specimen. It turns out that these coefficients decrease very quickly with distance between grains, so the sum in Eq. (11) can be limited to a finite number of neighboring grains.

Solution of (10) gives a strain value at any point of any grain provided that the subgrain volume around the point tends to 0.

Equations (11) have one important feature. The equation for $\varepsilon_{ij}^{(0)(a)(\xi)}$ in (11) includes the parameters only of the ξth grain. The equation for $\varepsilon_{ij}^{(1)(a)(\xi)}$ contains the parameters of all other ηth grains and has no parameters of the ξth grain. Thus, the zero- and first-order corrections $\varepsilon_{ij}^{(0)(a)(\xi)}$ and $\varepsilon_{ij}^{(1)(a)(\xi)}$ are statistically independent. The same is true for any two coefficients $\tilde{B}_{ijkl}^{(a\eta)}$ in the sum on the right-hand side of (11).

The product $\tilde{B}_{ijkl}^{(a\eta)}\varepsilon_{kl}^{*}$ represents the contribution of the interaction with the ηth grain, which is denoted by

$$\varepsilon_{ij}^{(1)(a)(\xi)}\Big|_\eta \equiv \tilde{B}_{ijkl}^{(a\eta)}\varepsilon_{kl}^{*}. \tag{13}$$

We rewrite the solution of (10) in the form of the sum of contributions:

$$\varepsilon_{ij}^{(a)(\xi)} \cong \varepsilon_{ij}^{(0)(a)(\xi)} + \sum_{\eta\neq\xi}\varepsilon_{ij}^{(1)(a)(\xi)}\Big|_\eta, \tag{14}$$

in which all terms on the right-hand side are statistically independent. Consequently, we can build separate distributions for $\varepsilon_{ij}^{(0)(a)(\xi)}$ and all contributions

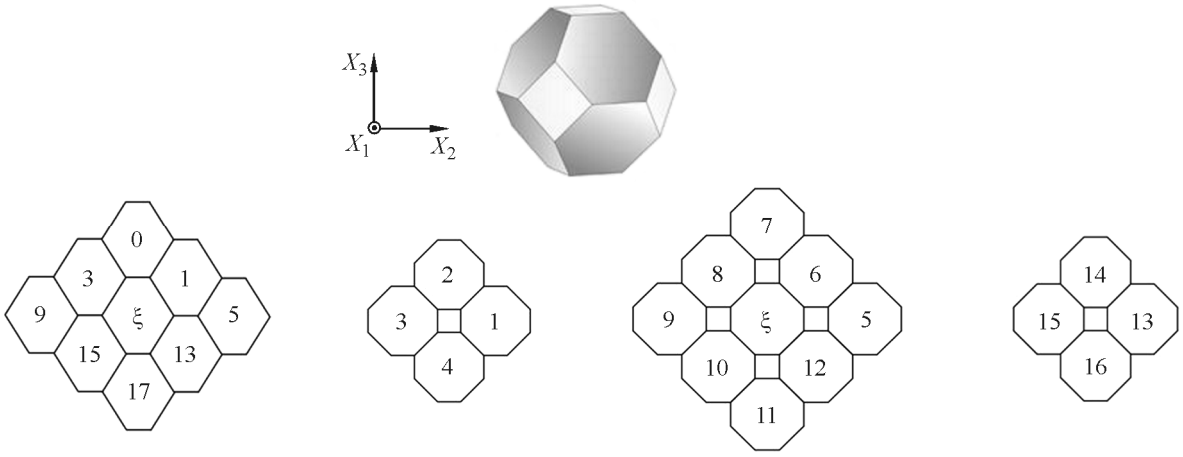

Fig. 1. Grain shape, vertical (left) and three horizontal sections of a model polycrystal.

$\varepsilon_{ij}^{(1)(a)(\xi)}|_{\eta}$ as well as the total distribution for $\varepsilon_{ij}^{(a)(\xi)}(\mathbf{r}_a)$ as the sum of independent random variables. This is a great computational advantage of the integral equation method.

4. NUMERICAL EXAMPLES OF MESOSTRAIN DISTRIBUTIONS

The approach described above is applicable to single-phase model polycrystals with grains in the form of truncated octahedra of equal volumes. Truncated octahedra continuously fill the space, closely resemble natural grains, simplify the construction of grain structure geometry, and are often used in numerical simulation. Perfect contact is specified at grain boundaries (continuity of the displacement vector, which is used in deducing integral Eq. (1) for the strain tensor). The grain boundary thickness is considered to be zero. Each grain has 18 nearest neighbors. Figure 1 shows the grain shape, a vertical and three characteristic horizontal sections of a 19 grain cluster (the central ξth grain is the grain to be studied) in the coordinate system, and numbers of the neighboring grains.

Consideration is given to an untextured polycrystal. Crystallographic axes of the grains are distributed randomly and uniformly in space. The latter means that all directions of the crystallographic axes (which are parallel to the axes of elastic symmetry of each grain) are equally probable. The crystallographic orientations of different grains are uncorrelated. Thus, a sufficiently large polycrystal is elastically isotropic on the macroscale. The summation in (11) is made over all grains in the polycrystal. The sum contains a very large number of terms. However, the coefficients $\tilde{B}_{ijmn}^{(a\eta)}$ quickly decrease with distance between grains, because Green's tensor decreases in inverse proportion to the cube of the distance $|\mathbf{r}_a - \mathbf{r}_\eta|^{-3}$. Therefore, as a first approximation, the sum is limited to the 18 nearest neighbors. The influence of more distant grains can easily be taken into account.

In numerical examples, a model polycrystal is loaded by uniaxial tension along the vertical X_3 axis. Uniaxial tension with the stress tensor component σ_{33} (the rest are equal to 0) corresponds to the kinematic boundary conditions $u_m(\mathbf{r})\big|_\Gamma = \varepsilon_{mn}^* x_n$ with the normal strain tensor components equal to $\varepsilon_{33}^* = \sigma_{33}/E$, $\varepsilon_{11}^* = \varepsilon_{22}^* = -\nu\varepsilon_{33}^*$ and shear ones equal to 0, where E and ν are Young's modulus and Poisson's ratio of a macroscopically isotropic polycrystal.

Let us set the task of calculating the probability density of the longitudinal (in the loading direction) mesostrain tensor component $\varepsilon_{33}^{(a)(\xi)} \cong \varepsilon_{33}^{(0)(a)(\xi)} + \varepsilon_{33}^{(1)(a)(\xi)}$ in the laboratory coordinate system of a polycrystal.

The analysis of the first equation in (11) shows that, for spherical grains, the zero-order correction is exactly homogeneous inside the grain [27]. For grains in the form of a truncated octahedron, the numerical calculation gives a homogeneous solution for zero-order corrections for all subgrains within 90% of the grain volume, being inhomogeneous only near the faces and edges (where elastic unphysical divergences and plastic shear strains arise). First-order corrections $\varepsilon_{ij}^{(1)(a)(\xi)}$ are inhomogeneous over the grain volume. We consider strains only in the bulk of grains.

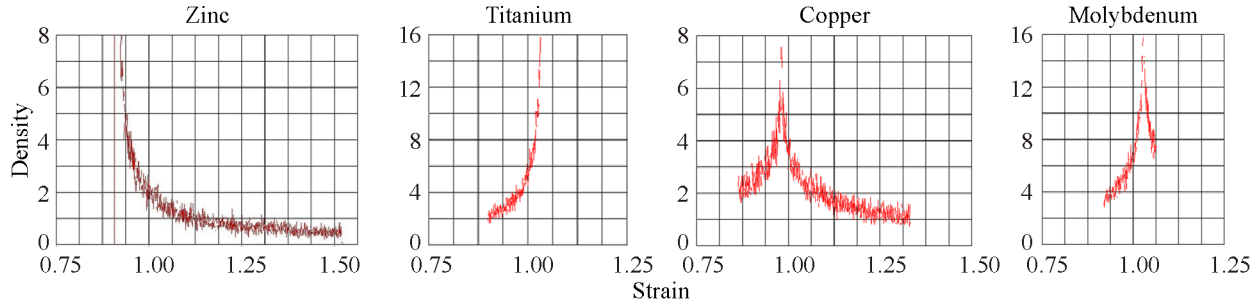

Fig. 2. Probability density of strains for zero-order corrections $\varepsilon_{33}^{(0)(a)(\xi)}$. The horizontal axis is the relative strain $\varepsilon_{33}^{(0)(a)(\xi)}/\varepsilon_{33}^{*}$ (color online).

In the used model, the randomness of the grain structure of polycrystals is reduced to random equally probable orientations of crystallographic axes of all grains. The crystallographic orientation is specified by Euler angles. The equally probable distribution of the axes corresponds to the joint probability density of the Euler angles φ, ψ, and θ in the form $f(\varphi,\psi,\theta)=1/(8\pi)\sin\theta$, where φ, ψ, and θ are the angles of proper rotation, precession, and nutation, respectively [28]. The sets of random Euler angles are specified using a random number generator.

With 10^6 random crystallographic orientations for each grain, the dataset includes 10^6 elements for the zero-order correction $\varepsilon_{ij}^{(0)(a)(\xi)}$ and for 18 contributions $\varepsilon_{ij}^{(1)(a)(\xi)}|_{\eta}$ from the nearest neighbor interactions. All these variables are statistically independent. First, the distribution functions for these random contributions are derived separately. Since the datasets are discrete, the distribution functions are nondecreasing piecewise constant functions. Then, the probability densities for these 19 random variables are calculated by finite-difference differentiation of the distribution functions. The total probability density for $\varepsilon_{33}^{(a)(\xi)}$ is found by the laws of probability for the sum of these 19 statistically independent densities.

Calculations were performed for single-phase polycrystals with hexagonal and cubic elastic symmetries as well as with low and high anisotropy of grains: zinc (strong anisotropy with the lattice parameter ratio $c/a=1.856$), titanium (weak anisotropy with $c/a=1.587$), copper (strong anisotropy with the Zener factor 3.277), and molybdenum (weak anisotropy with the Zener factor 0.707). The elastic constants of single crystals and polycrystals are taken from [29, 30]. All figures below correspond to the central point of the ξth grain. For the rest points within 90% of the ξth grain volume, the results change slightly (5–6% variation).

Figure 2 shows the probability densities for zero-order corrections $\varepsilon_{33}^{(0)(a)(\xi)}$. The zero-order approximation is a solution for individual grains embedded in a homogenized medium. Thus, these curves are also strain distributions for isolated anisotropic randomly oriented Eshelby inclusions [27].

Figure 3 shows typical probability densities for first-order corrections $\varepsilon_{33}^{(1)(a)(\xi)}|_{\eta=6}\equiv\tilde{B}_{33kl}^{(a\eta)}\varepsilon_{kl}^{*}$ to the interaction with one nearest neighboring grain (number 6).

The behavior of the curves reflects the complex dependence of the interaction of grains on the mutual orientation of their crystallographic axes.

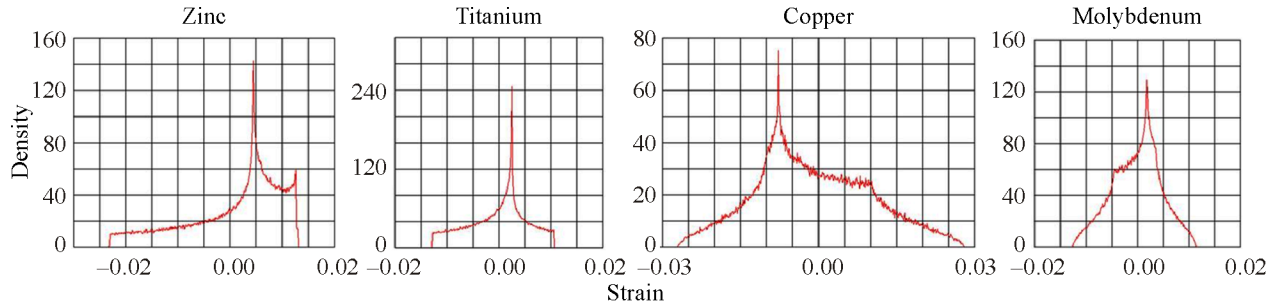

Fig. 3. Probability density of strains for the contribution from the interaction with grain 6. The horizontal axis is the relative strain $\varepsilon_{33}^{(1)(a)(\xi)}|_{\eta=6}/\varepsilon_{33}^{*}$ (color online).

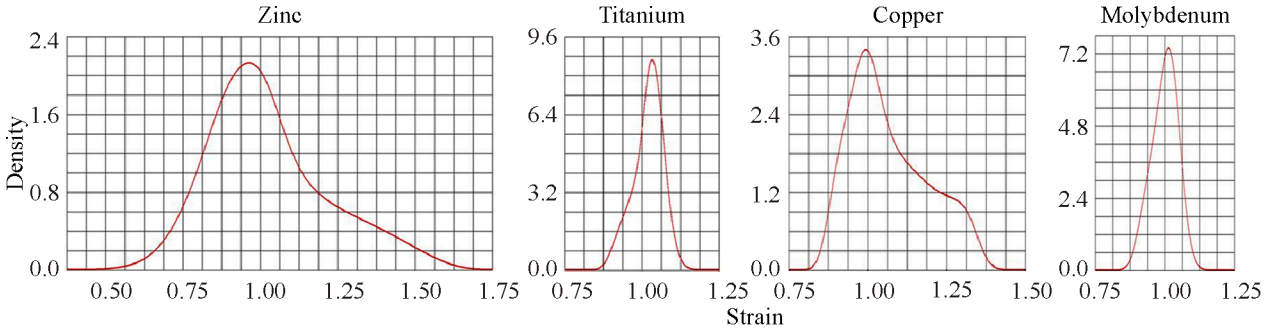

Fig. 4. Total probability densities. The horizontal axis is the relative strain $\varepsilon_{33}^{(a)(\xi)}/\varepsilon_{33}^{*}$ (color online).

Figure 4 shows the total probability densities of the strain components $\varepsilon_{33}^{(a)(\xi)}$. Numerical differentiation causes the sawtooth shape of the curves in Figs. 2 and 3. Summing the probability densities for $\varepsilon_{ij}^{(0)(a)(\xi)}$ and 18 contributions $\varepsilon_{ij}^{(1)(a)(\xi)}|_{\eta}$ smoothes the curves for the total probability densities in Fig. 4.

The contributions of different neighboring grains vary significantly. For example, in copper, the maximum contribution $\varepsilon_{33}^{(1)(a)(\xi)}|_{\eta}$ is from grain 0 (and is equivalent to 17), and the minimum contribution is from grain 5 (being equal to the contributions from grains 2, 3, 4, 13, 14, 15, and 16). The ratio of these contributions is 4.01. The contributions of other grains lie between these limiting values. Thus, only two grains (0 and 17 in a favorable orientation) can significantly increase the strain in the central ξth grain. In other polycrystals, the maximum influence can be exerted by other grains. The same is true for various types of external loads.

All probability densities are asymmetric and correspond to finite intervals of possible strains. The asymmetry is determined by the type of elastic anisotropy of single crystals and specific values of the elastic modulus tensor components of the grain. The higher the anisotropy of grains, the higher the asymmetry of the distribution. For polycrystals with very weak grain anisotropy (such as tungsten with the Zener factor 1), the probability density reduces to the Dirac delta function. The average strain and the stain with the highest probability are not the same. The distribution tails tend to 0 at the boundaries of the definition domain exponentially. On the scale of Fig. 4, these tails are invisible. For example, the maximum possible relative strain for zinc is equal to $\varepsilon_{33}^{(a)(\xi)}/\varepsilon_{33}^{*}=1.92$, which is almost twice the macrostrain. For this polycrystal with the relative strain more than 1.5, the probability of mesostrain is about 0.02. This probability is large enough to be a possible cause of triggering critical local events (such as primary damage).

The asymmetry of the distributions is also governed by the large difference in the zero- and first-order corrections. From Fig. 2 it can be seen that, for zinc, the maximum contribution of the zero-order correction is more than 10 times higher than that of the first-order correction to the interaction with grain 6 shown in Fig. 3. The total maximum influence of all nearest neighbors is comparable to the zero-order correction, but has a very low probability, because it requires that these neighbors be simultaneously oriented in specific extreme positions. Therefore, for zinc, the long tail of the probability density with the zero-order corrections towards high strains leads to the asymmetry of the central region of the total probability density in Fig. 4. Similar considerations qualitatively illustrate the asymmetry of the probability density for copper. For polycrystals with weak elastic anisotropy of grains, the zero- and first-order corrections are comparable. As a result, the strain distribution densities for titanium and molybdenum are almost symmetric, being close to the normal distribution.

If the polycrystal deformation passes to the plastic region, the distributions change. It is obvious that the left and right tails of the probability density should be differently elongated due to the fact that the plastic part of the total tensile strain will have mainly positive values. Some authors use the lognormal distribution to interpolate the total strain at the plastic stage, but assume that the elastic part of deformation remains normally distributed [19].

Taking into account interactions with the second, third and subsequent neighbors hardly changes the behavior of the elastic probability densities, but fur-

ther increases the limiting values. With consideration for the interactions with the nearest (18 grains), second (66 grains) and third (146 grains) neighbors, the maximum relative strain is 2.75 for zinc. This value of the limiting strain corresponds to a certain crystallographic orientation of a sufficiently large number of grains. In an untextured polycrystal with equally probable orientations of crystallographic axes of grains, the formation of such a cluster of grains has a very low probability, but is of theoretical interest.

In polycrystals with high grain anisotropy, the maximum possible strain is more than 2 times higher than the macroscopic one. Neighboring grains in configurations with the maximum contribution to the strain of a given grain constitute clusters of an extreme grain structure described in [31, 32], which often present sources of damage.

5. CONCLUSIONS

The method proposed for plotting the probability densities of strain is based on specific mathematical features of the integral form of the boundary value problem of deformation of polycrystalline materials. The integral equation for strains (1) is completely equivalent to the differential formulation of the boundary value problem, consisting of equilibrium equations in displacements and boundary conditions, and was deduced from the latter by correct mathematical procedures [23–25]. The advantage of the integral method is that the solution to the boundary value problem of a polycrystalline solid is considered as a result of grain interactions. Contributions from these interactions are additive and statistically independent in the first order of the intensity of interactions. Thus, it was revealed that the influence of interactions with different neighbors on the strain state of the studied grain differed significantly, sometimes by an order.

The property of additivity allowed obtaining large statistical samples of random variables. They are important for finding extreme values of the strain tensor components that define distribution boundaries and correspond to the simultaneous low-probability orientation of a group of grains in certain positions. A sample of 10^6 different orientations for the central grain and for each of the 18 nearest neighbors corresponds to $10^{6\times19}$ random implementations of the local grain structure. The probability of random formation of an extreme cluster of 19 grains is of the order of p^{19} (p is the probability of orientation of each grain in an extreme position). This is a very low probability. From the qualitative viewpoint, the proposed method provides sufficient statistics of random strains to build a continuous distribution, including the distribution boundaries. The non-Gaussian type of the distributions is associated with a large difference in the intensities of interactions with neighboring grains, which are differently located relative to the studied grain and external loading directions. In addition, the number of interacting neighboring grains is limited and insufficient to apply the central limit theorem of probability theory.

The aim of the work was to study the influence of random grain interactions caused by their different crystallographic orientations on the statistics of random mesostrains. For this purpose, calculations were made on model polycrystals with grains in the form of truncated octahedra. The method is also applicable to other grain models built using Voronoi polyhedra or by other methods, but it requires large computational resources.

The proposed method provides a rapid calculation of distributions of strain components under various conditions of multiaxial macroloading. It is easily transformed for stress distributions (according to Hooke's law) and can be used to estimate the probabilities of critical mechanical events in polycrystalline materials.

FUNDING

The work was carried out within the government statement of fundamental scientific research (line FSNM-2023-006).

CONFLICT OF INTEREST

The authors of this work declare that they have no conflicts of interest.

REFERENCES

1. McCormick, N. and Lord, J., Digital Image Correlation, *Mater. Today*, 2010, vol. 13, no. 12, pp. 52–54. https://doi.org/10.1016/S1369-7021(10)70235-2
2. Pan, B., Qian, K., Xie, H., and Asundi, A., Two-Dimensional Digital Image Correlation for In-Plane Displacement and Strain Measurement: A Review, *Meas. Sci. Technol*., 2009, vol. 20, no. 6, p. 062001. https://doi.org/10.1088/0957-0233/20/6/062001
3. Henningson, A., Wills, A., Hall, S., Hendriks, J., Wright, J., Schon, T., and Poulsen, H., Inferring the Probability Distribution over Strain Tensors in Polycrystals from Diffraction Based Measurements, *Comp. Meth. Appl. Mech. Eng. A*, 2023, vol. 417, p. 116417.
4. Ludwig, W., Herbig, M., Buffiere, J.Y., Reischig, P., King, A., and Proudhon, H., Characterization of Polycrys-

talline Materials by X-Ray Diffraction Contrast Tomography, *MECAMAT 2010—Nouvelles Approches en Mecanique des Materiaux, Aussois, France*, 2010, hal-00534494.
5. McDonald, S.A., Reischig, P., Holzner, C., Lauridsen, E.M., Withers, P.Y., Merkle, A.P., and Feser, M., Non-Destructive Mapping of Grain Orientations in 3D by Laboratory X-Ray Microscopy, *Sci. Rep*., 2015, vol. 5, p. 14665. https://doi.org/10.1038/srep14665
6. Ludwig, W., Herbiga, M., King, A., Reischigd, P., Proudhone, H., and Buffièrea, J.Y., The Grain Microstructure of Polycrystalline Materials as Revealed by the Combined Use of Synchrotron X-Ray Imaging and Diffraction Techniques, *J. Annuelles de la SF2M*, 2010, hal-00534 495.
7. Miller, M.P., Pagan, D.C., Beaudoin, A.J., Nygren, K.E., and Shadle, D.J., Understanding Micromechanical Material Behavior Using Synchrotron X-Rays and In Situ Loading, *Metall. Mater. Trans. A*, 2020, vol. 51, pp. 4360–4376. https://doi.org/10.1007/s11661-020-05888-w
8. Schuren, J.C., Shade, P.A., Bernier, J.V., Li, S.F., Blank, B., Lind, J., Kenesei, P., Lienert, U., Suter, R.M., Turner, T.J., Dimiduk, D.M., and Almer, J., New Opportunities for Quantitative Tracking of Polycrystal Responses in Three Dimensions, *Curr. Opin. Solid State Mater. Sci*., 2014, vol. 19, pp. 235–244. https://doi.org/10.1016/j.cossms.2014.11.003
9. Benedetti, I. and Barbe, F., Modelling Polycrystalline Materials: An Overview of Three-Dimensional Grain-Scale Mechanical Models, *J. Multiscale Modelling*, 2014, vol. 5, pp. 1350002-1–1350002-51.
10. Bargmann, S., Klusemann, B., Markmann, J., Schnabel, J., Schneider, K., Soyarslan, C., and Wilmers, J., Generation of 3D Representative Volume Elements for Heterogeneous Materials: A Review, *Progr. Mater. Sci*., 2018, vol. 96, pp. 322–384.
11. Romanova, V. and Balokhonov, R., A Method of Step-By-Step Packing and Its Application In Generating 3D Microstructures of Polyrystalline and Composite Materials, *Eng. Computers*, 2021, vol. 37, pp. 241–250.
12. Quey, R. and Renversade, L., Optimal Polyhedral Description of 3D Polycrystals: Method and Application to Statistical and Synchrotron X-Ray Diffraction Data, *Comp. Meth. Appl. Mech. Eng*., 2018, vol. 330, pp. 308–333.
13. Balokhonov, R.R., Sergeev, M.V., and Romanova, V.A., Simulation of Deformation and Fracture in Polycrystalline Aluminum Alloy under Dynamic Loading, *Phys. Mesomech*., 2023, vol. 26, no. 3, pp. 267–281. https://doi.org/10.1134/S1029959923030037
14. Balokhonov, R., Romanova, V., and Kulkov, A., Microstructure-Based Analysis of Deformation and Fracture in Metal-Matrix Composite Materials, *Eng. Failure Analysis*, 2020, vol. 110, p. 104412.
15. Dawson, P.R., Miller, M.P., Pollock, T.M., Wendorf, J., Mills, L.H., Stinville, J.Ch., Charpagne, M.A., and Echlin, M.P., Mechanical Metrics of Virtual Polycrystals (MechMet), *Integr. Mater. Manuf. Innov*., 2021, vol. 10, pp. 265–285.
16. Trusov, P.V. and Shveikin, A.I., *Multilevel Models of Single-Crystal and Polycrystalline Materials: Theory, Algorithms, Examples of Application*, Novosibirsk: SB RAS Publ. House, 2019.
17. Hayashi, Y., Setoyama, D., Hirose, Y., Yoshida, T., and Kimura, H., Intragranular Three-Dimensional Stress Tensor Fields in Plastically Deformed Polycrystals, *Science*, 2019, vol. 366, pp. 1492–1496. https://doi.org/10.1126/science.aax9167
18. Guerchais, R., Morel, F., and Saintier, N., Effect of Defect Size and Shape on the High-Cycle Fatigue Behavior, *Int. J. Fatigue*, 2017, vol. 100, pp. 530–539. https://doi.org/10.1016/j.ijfatigue.2016.12.010
19. Chen, J., Wang, Z., and Korsunsky, A.M., Multiscale Stress and Strain Statistics in the Deformation of Polycrystalline Alloys, *Int. J. Plast*., 2022, vol. 152, p. 103260. https://doi.org/10.1016/j.ijplas.2022.103260
20. Bretin, R., Levesque, M., and Bocher, P., Neighborhood Effect on the Strain Distribution in Linearly Elastic Polycrystals: Part 1—Finite Element Study of the Interaction between Grains, *Int. J. Solids Struct*., 2019, vol. 176–177.
21. Zinovieva, O.S., Mechanical Aspects of Mesoscale Deformation-Induced Surface Roughening in Loaded Polycrystals, *Cand. Sci (Phys.-Math) Dissertation*, Tomsk: TSU, 2015.
22. Abdolvand, H., Wright, J., and Wilkinson, A.J., Strong Grain Neighbour Effects in Polycrystals, *Nat. Commun*., 2018, vol. 9, p. 171.
23. deWit, R., Continuum Theory of Stationary Dislocations, in *Solid State Physics. Advances in Research and Applications*, vol. 10, New York: Academic Press Inc., 1960.
24. Shermergor, T.D., *Theory of Elasticity of Microinhomogeneous Media*, Moscow: Nauka, 1977.
25. Mura, T., *Micromechanics of Defects in Solids*, Dordrecht: Nijhoff, 1987.
26. Shavshukov, V. and Tashkinov, A., Quantum Field Theory Approach to Mechanics of Polycrystals, *Solid State Phenom*., 2016, vol. 243, pp. 131–138.
27. Tashkinov, A. and Shavshukov, V., Inhomogeneities in Grains of Polycrystalline Materials and Eshelby Problem, *PNRPU Mech. Bull.*, 2018, no. 1, pp. 58–72.
28. Tashkinov, A.A. and Shavshukov, V.E., Extreme Clusters of Grains in Random Microstructure of Polycrystals, *PNRPU Mech. Bull.,* 2021, no. 2, pp. 153–166.
29. Bogachev, I.N., Vainshtein, A.A., and Volkov, S.D., *Statistical Metallurgy*, Moscow: Metallurgiya, 1984.
30. Simmons, G. and Wang, H., *Single Crystal Elastic Constants and Calculated Aggregate Properties: A Handbook*, Cambridge, Mass.: The M.I.T. Press, 1971.
31. Huntington, H.B., The Elastic Constants of Crystals, in *Solid State Physics. Advances in Research and Applications, vol. 7*, New York: Academic Press Inc., 1958.
32. Miao, J., Pollock, T.M., and Jones, J., Microstructural Extremes and the Transition from Fatigue Crack Initiation to Small Crack Growth in a Polycrystalline Nickel-Base Superalloy, *Acta Mater*., 2012, vol. 60, pp. 2840–2854. https://doi.org/10.1016/j.actamat.2012.01.049